International Symposium
On Turbulence and Shear Flow
Phenomena (TSFP-9)
June 30 - July 3, 2015 *Melbourne, Australia*

DNS OF THERMALLY-STRATIFIED TURBULENT BOUNDARY LAYERS SUBJECTED TO ADVERSE PRESSURE GRADIENT

H. Hattori, A. Kono, T. Houra and M. Tagawa
Department of Mechanical Engineering
Nagoya Institute of Technology
Gokiso-cho, Showa-ku, Nagoya 466-855, JAPAN
hattori@nitech.ac.jp

ABSTRACT

The objective of this study is to investigate and observe turbulent heat transfer structures and statistics in thermally-stratified turbulent boundary layers subjected to a non-equilibrium adverse pressure gradient (APG) by means of direct numerical simulation (DNS). DNSs are carried out under conditions of neutral, stable and unstable thermal stratifications with a non-equilibrium APG, in which DNS results reveal heat transfer characteristics of thermally-stratified non-equilibrium APG turbulent boundary layers. In cases of thermally-stratified turbulent boundary layers affecting APG, heat transfer performances increase in comparison with a turbulent boundary layer with neutral thermal stratification and zero pressure gradient. The characteristic turbulent statistics of both the velocity and the thermal fields along streamwise direction are clearly indicated, in which the decrease of log-law profile of streamwise mean velocity which was found by experimental study is also observed in the neutral boundary layer of our DNS. DNS results reveal that the turbulent characteristics of both cases of stable and unstable thermal stratifications boundary layers are different to the turbulent characteristics of the neutral boundary layer having APG.

INTRODUCTION

Since a turbulent boundary layer subjected to an adverse pressure gradient (APG) which is yielded by increase of pressure toward streamwise direction and also causes the flow separation, affects the turbulent structure and heat transfer strongly, a turbulent heat transfer phenomenon of APG flow should be explored for the controls of flow and heat transfer. APG turbulent boundary layer with heat transfer has been revealed by the experimental (Nagano *et al.*, 1993, 1998; Houra & Nagano, 2006) and DNS (Lee & Sung, 2008; Araya & Castillo, 2013) studies. On the other hand, a thermally-stratified turbulent boundary layer which can be observed in the atmosphere has been also investigated by the experimental (Ohya, 2001) and DNS (Hattori *et al.*, 2007, 2014) studies, which expand the understanding of turbulent structure in a thermally-stratified turbulent boundary layer. Although by those studies, the detailed researches for structures of turbulent heat transfer have been proceeding, a study for turbulent boundary layer with overlapping of several influencing factors in turbulent structures such as thermal stratifications and pressure gradients is needed in order to know a mechanism of more complex turbulent heat transfer. Thus, a turbulent heat transfer subjected to thermal stratification and pressure gradient should be explored as the typical situation.

In this study, in order to investigate and observe effects of adverse pressure gradient for a thermally-stratified turbulent boundary layer, DNS of thermally-stratified turbulent boundary layers subjected to adverse pressure gradient is carried out, where a non-equilibrium APG turbulence flow is assumed and various thermally-stratified turbulent boundary layers with a non-equilibrium APG are simulated in order to reveal statistics and structures in such fields.

DNS OF THERMALLY-STRATIFIED TURBULENT BOUNDARY LAYER WITH APG

Assuming that the Boussinesq approximation is approved for the Navier-Stokes equation, the governing equations used in the present DNS are indicated as follows (Hattori *et al.*, 2007):

$$\frac{\partial u_i}{\partial t} + u_j \frac{\partial u_i}{\partial x_j} = -\frac{\partial p}{\partial x_i} + \frac{1}{Re_{\delta_{2,\mathrm{in}}}} \frac{\partial^2 u_i}{\partial x_j \partial x_j} + \delta_{i2} Ri_{\delta_{2,\mathrm{in}}} \theta \quad (1)$$

$$\frac{\partial u_i}{\partial x_i} = 0 \quad (2)$$

$$\frac{\partial \theta}{\partial t} + u_j \frac{\partial \theta}{\partial x_j} = \frac{1}{Pr\, Re_{\delta_{2,\mathrm{in}}}} \frac{\partial^2 \theta}{\partial x_j \partial x_j} \quad (3)$$

where the Einstein summation convention applies to repeated indices, and a comma followed by an index indicates differentiation with respect to the indexed spatial coordinate. u_i^* is the dimensionless velocity component in x_i direction, θ^* is the dimensionless temperature difference, p^* is the dimensionless pressure, t^* is the dimensionless time, and x_i^* is the dimensionless spatial coordinate in the i direction, respectively. $Re_{\delta_{2,\mathrm{in}}} = \bar{U}_0 \delta_{2,\mathrm{in}} / \nu$ is the Reynolds number based on the free stream velocity and the momentum thickness at the inlet of the driver part, $\delta_{2,\mathrm{in}}$. Note that "the driver part" means the inflow data generator for the inlet boundary of the main simulation part (Hattori *et al.*, 2007). $Pr = \nu/\alpha$ is the Prandtl number, and $Ri_{\delta_{2,\mathrm{in}}} = g\beta\delta_{2,\mathrm{in}}\Delta\Theta/\bar{U}_0^2$ is the bulk Richardson number based on the free stream velocity, the momentum thickness at the inlet of the driver part, and the temperature difference between a free stream and a wall ($\Delta\Theta = \bar{\Theta}_0 - \bar{\Theta}_w$). In the governing equations, the dimensionless variables are given using the free stream velocity, $\bar{U}_0$, and the free stream

temperature, Θ_0, at the inlet of the driver part, and the wall temperature, Θ_w.

The Prandtl number is set to 0.71, assuming the working fluid to be air. The Reynolds number is set to 300, and the Richardson numbers are set to -0.003 (unstable thermal stratification boundary layer: UBL), 0 (neutral thermal stratification boundary layer: NBL) and 0.05 (stable thermal stratification boundary layer: SBL).

For efficiently conducting the DNS of thermally-stratified turbulent boundary layers subjected to APG, the computational domain is composed of two parts; one is the driver part where a zero-pressure-gradient (ZPG) flow with an isothermal wall is generated and used as the inflow boundary condition for the main simulation, and the other is the main part where a thermally-stratified turbulent boundary layers subjected to adverse pressure gradient are simulated. A central finite-difference method of second-order accuracy is used to solve the equations of continuity, momentum and energy (Hattori & Nagano, 2004; Hattori *et al.*, 2007), where the computational domain is arranged as $x \times y \times z = 600\delta_{2,\mathrm{in}} \times 30\delta_{2,\mathrm{in}} \times 40\delta_{2,\mathrm{in}}$ for the conditions of neutral and stable thermal stratifications, and $x \times y \times z = 600\delta_{2,\mathrm{in}} \times 60\delta_{2,\mathrm{in}} \times 40\delta_{2,\mathrm{in}}$ for the conditions of unstable thermal stratification due to the increase of boundary layer thickness. The grid points are given as $x \times y \times z = 1152 \times 128 \times 128$ in the neutral and SBL conditions, and $x \times y \times z = 1152 \times 160 \times 128$ in the UBL condition for the main part of DNS.

In order to achieve APG condition in the free stream, the boundary conditions of free stream are given as follows:

$$\frac{\partial u}{\partial y} = 0, \quad \frac{\partial w}{\partial y} = 0, \quad \frac{\partial v}{\partial y} = -\frac{\partial u}{\partial x} - \frac{\partial w}{\partial z} \tag{4}$$

$$\bar{U}_e(x) = \bar{U}_0 \sqrt{1 - C_p(x)} \tag{5}$$

where u, v and w are velocities in streamwise (x), wall-normal (y) and spanwise (z) directions, respectively. $\bar{U}_e(x)$ is a local mean free stream velocity, $C_p = (P(x) - P(0))/(\rho \bar{U}_0/2)$ is the local pressure coefficient, $P(x)$ is a local mean pressure, and $P(0)$ is the free stream pressure at the inlet. C_p is set to 0 at the inlet of main part of DNS, and C_p is increased along the streamwise direction. Finally, C_p reaches 0.2 at the out let of main part of DNS in order to achieve the APG flow. For the ZPG flow, $C_p(x)$ is set to 0. The non-slip condition for velocity field and the isothermal condition for thermal field at the wall, and the convective boundary condition (Hattori *et al.*, 2007) at the outlet and the periodic condition for the spanwise direction are adopted for both velocity and thermal fields.

On the other hand, the Reynolds-averaged Navier-Stokes equations as indicated in Eq. (1) are given as follows:

$$\bar{U}\frac{\partial \bar{U}}{\partial x} + \bar{V}\frac{\partial \bar{U}}{\partial y} = -\frac{\partial \bar{P}}{\partial x} + \frac{\partial}{\partial x}\left(\frac{1}{Re_{\delta_{2,\mathrm{in}}}}\frac{\partial \bar{U}}{\partial x} - \overline{u^2}\right) + \frac{\partial}{\partial y}\left(\frac{1}{Re_{\delta_{2,\mathrm{in}}}}\frac{\partial \bar{U}}{\partial y} - \overline{uv}\right) \tag{6}$$

$$\bar{U}\frac{\partial \bar{V}}{\partial x} + \bar{V}\frac{\partial \bar{V}}{\partial y} = -\frac{\partial \bar{P}}{\partial y} + \frac{\partial}{\partial x}\left(\frac{1}{Re_{\delta_{2,\mathrm{in}}}}\frac{\partial \bar{V}}{\partial x} - \overline{uv}\right) + \frac{\partial}{\partial y}\left(\frac{1}{Re_{\delta_{2,\mathrm{in}}}}\frac{\partial \bar{V}}{\partial y} - \overline{v^2}\right) + Ri_{\delta_{2,\mathrm{in}}}\theta \tag{7}$$

where $\bar{U}$ and $\bar{V}$ are mean velocities in streamwise and wall-normal directions, respectively. The spanwise mean velocity vanishes due to the assumption of 2-dimensional mean flow field. Considering these equations, note that the effect of APG mainly affects the momentum equation of streamwise direction and the effect of thermal stratification remarkably acts on the momentum equation of wall-normal direction.

RESULTS AND DISCUSSION

Fundamental Parameters

Figures 1, 2 and 3 show the local friction coefficients, C_f, the local Stanton numbers, St, and the ration between C_f and St, respectively. Here, the remarkable decrease of C_f along the streamwise direction is found in case of SBL with APG, and C_f comes close to zero near $x/\delta_{2,\mathrm{in}} = 500$ as shown in Fig. 1. However, C_f does not become zero, and then C_f again increases in the adopting domain in the streamwise direction as $x = 600\delta_{2,\mathrm{in}}$. Since it is considered that the re-increase may be caused by the effect of domain size, DNS of the expanding domain in the streamwise direction as $x = 900\delta_{2,\mathrm{in}}$ is carried out for killing the effect of domain size. As the result, the effect of domain size does not affect the behavior of C_f as shown in Fig. 1. Thus, the separation of flow is not observed in case of SBL with APG, but the flow separation is slightly found in the instantaneous field. The local friction coefficients of APG generally decreases in comparison with those of ZPG in all cases. The local Stanton numbers of APG are larger than those of ZPG as indicated in Fig. 2. Therefore, the ratios between C_f and St of APG in all cases become smaller than those of ZPG as shown in Fig. 3, i.e., the efficiency of heat transfer is enhanced due to the effect of APG, although the effect of SBL also enhances the efficiency of heat transfer.

Turbulent Statistics for Velocity Field

The profiles of turbulent statistics normalized by both the inner and outer scales for velocity field are shown in Figs. 4$\sim$ 7. The typical profile of streamwise mean velocity normalized by inner scale in case of NBL with APG (Nagano *et al.*, 1993, 1998; Houra & Nagano, 2006) is shown in Fig. 4(a), in which the standard log-law profile is not maintained due to the effect of APG and the wake region is raised up. Since the inner scale in case of SBL with APG significantly varies, the remarkably changing profiles of mean velocity are observed as shown in Fig. 4(b). On the other hand, the decrases of mean velocity in the log-law region are found in case of UBL, but the wake region is not raised up as indicated in Fig. 4(c). In all cases, the deceleration of mean velocity normalized by outer scale due to APG is found in the outer and free stream regions, but the different behaviors of mean velocity can be clearly seen in the inner region.

The Reynolds shear stress is demonstrated in Fig. 5. In case of NBL, the increase of Reynolds shear stress normalized by inner scale is observed along the streamwise di-

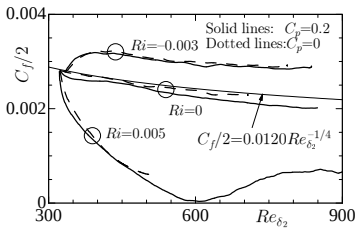

(a) vs. Re_{δ_2}

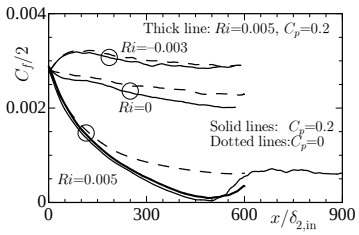

(b) vs. $x/\delta_{2,\mathrm{in}}$

Figure 1. Local friction coefficients

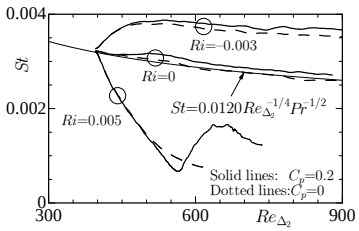

(a) vs. Re_{δ_2}

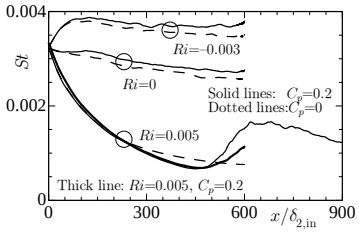

(b) vs. $x/\delta_{2,\mathrm{in}}$

Figure 2. Local Stanton numbers

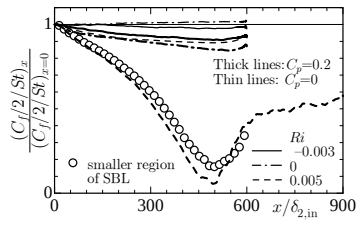

Figure 3. Ratios between C_f and St

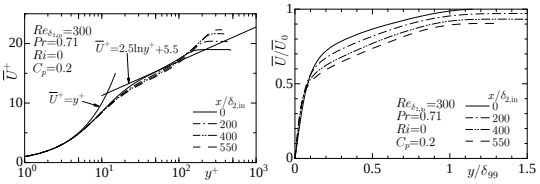

(a) Neutral stratification

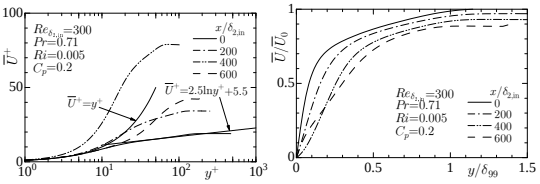

(b) Stable stratification

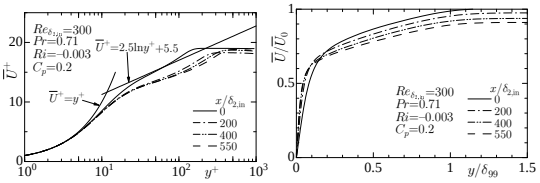

(c) Unstable stratification

Figure 4. Profiles of streamwise mean velocity; right side: inner scale, left side: outer scale

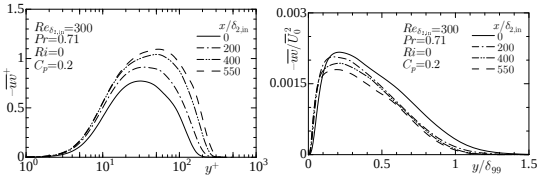

(a) Neutral stratification

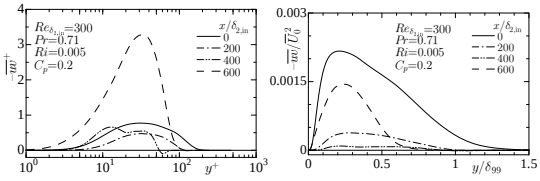

(b) Stable stratification

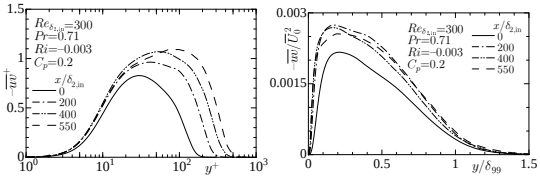

(c) Unstable stratification

Figure 5. Profiles of Reynolds shear stress; right side: inner scale, left side: outer scale

rection, but the decrease of the net Reynolds shear stress can be found by the outer scale normalization. Although the Reynolds shear stress remarkably decreases toward the

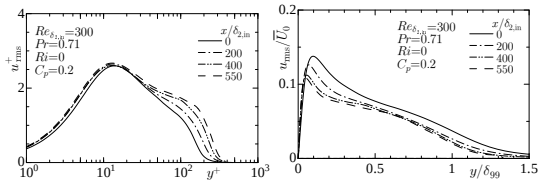

(a) Neutral stratification

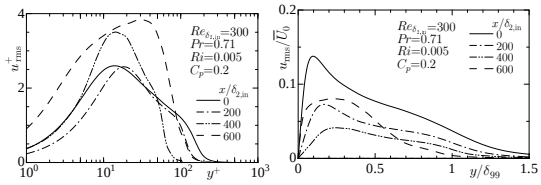

(b) Stable stratification

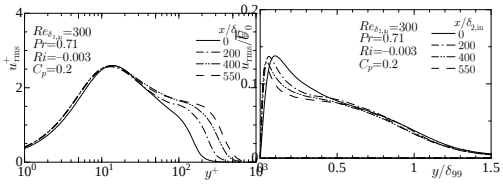

(c) Unstable stratification

Figure 6. Profiles of streamwise rms velocity fluctuation; right side: inner scale, left side: outer scale

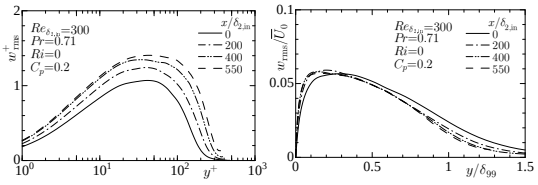

(a) Neutral stratification

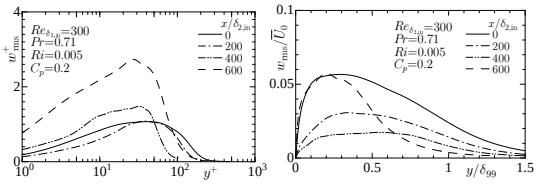

(b) Stable stratification

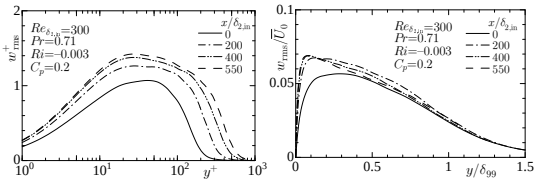

(c) Unstable stratification

Figure 8. Profiles of spanwise rms velocity fluctuation; right side: inner scale, left side: outer scale

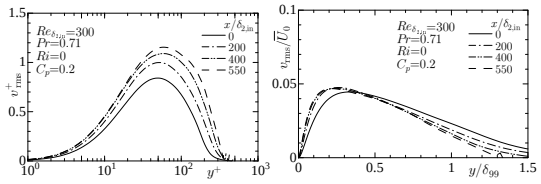

(a) Neutral stratification

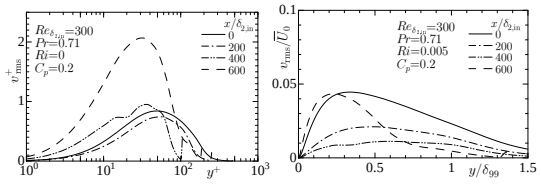

(b) Stable stratification

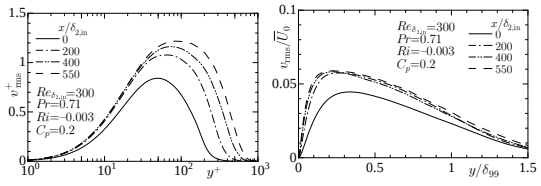

(c) Unstable stratification

Figure 7. Profiles of wall-normal rms velocity fluctuation; right side: inner scale, left side: outer scale

streamwise direction in case of SBL, it can be seen that the Reynolds shear stress is re-grown in the downstream region. Therefore, the local friction coefficient again increases in the downstream region as shown in Fig. 1. In case of UBL, the increase of Reynolds shear stress normalized by inner scale can be also seen, but the Reynolds shear stress normalized by outer scale also increases, which is different phenomenon in comparison with case of NBL. Thus, the different profiles of mean velocity can be observed as shown in Fig. 4(c).

The rms velocity fluctuations in streamwise, wall-normal and spanwise directions are shown in Figs. 6∼ 8. In case of NBL, the streamwise rms velocity fluctuation normalized by inner scale, u^+_{rms}, hardly changes near the wall, but the wall-normal rms velocity fluctuation normalized by inner scale, v^+_{rms}, significantly increases. However, it can be seen that the wall-normal rms velocity fluctuation normalized by outer scale, $u^*_{\mathrm{rms}}(= u_{\mathrm{rms}}/\bar{U}_0)$, hardly varies as shown in the right side of Figs. 7(a), but the decrease of streamwise rms velocity fluctuation normalized by outer scale, $v^*_{\mathrm{rms}}(= v_{\mathrm{rms}}/\bar{U}_0)$, is observed as indicated in the right side of Fig. 6(a). In case of SBL, both u^*_{rms} and v^*_{rms} decrease along the streamwise direction, and then the rms velocity fluctuations are re-generated near the wall. Especially, it can be observed in the right side of Fig. 7 that the near-wall v^*_{rms} is rapidly generated. Thus, the Reynolds shear stress in case of SBL as shown in Fig. 4(b) is also re-generated with yielding v^*_{rms} at $x/\delta_{2,\mathrm{in}} = 600$ where the friction coefficient again increases. As for case of UBL, it can be seen that u^+_{rms} remarkably increases in the outer region, but decreases of u^*_{rms} are observed near the wall. On the other hand, increases of both v^+_{rms} and v^*_{rms} can be seen as shown in Fig. 7(c) due to the effect of thermal stratification which directly affects the wall-normal velocity as indicated in Eq. (7). As for the spanwise rms velocity fluctuation w_{rms}, tendencies of profiles of w_{rms} in all cases are sim-

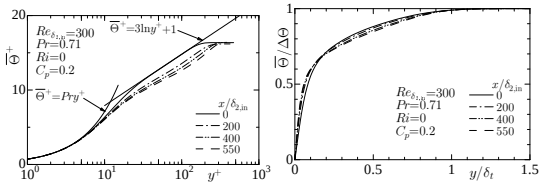

(a) Neutral stratification

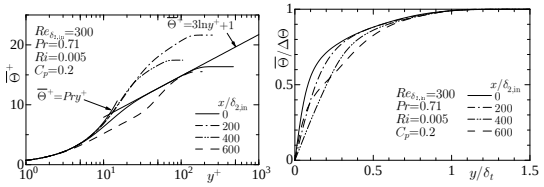

(b) Stable stratification

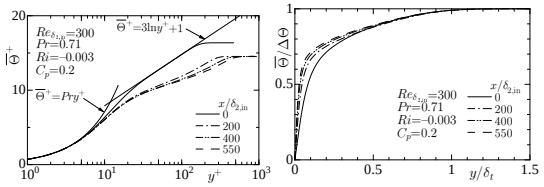

(c) Unstable stratification

Figure 9. Profiles of mean temperature; right side: inner scale, left side: outer scale

ilar to tendencies of profiles of v_{rms}, but it can be found that w^{+}_{rms} remarkably increases in the vicinity of wall in cases of both NBL and UBL in comparison with v^{+}_{rms}.

Turbulent Statistics for Thermal Field

Turbulent statistics in thermal field are shown in Fig. 9$\sim$ 12. Profiles of mean temperature are demonstrated in Fig. 9. As for the profiles normalized by inner scale, $\tilde{\Theta}^{+}$, only decrease of mean temperature in log-law region can be seen in case of NBL, but the maximum value of $\tilde{\Theta}^{+}$ does not change, because the ratio between Cf and St hardly varies in case of NBL where the maximum value of $\tilde{\Theta}^{+}$ is proportional to $1/\theta_{\tau}$ that is $\sqrt{Cf/2}/St$. Hence, the maximum value of $\tilde{\Theta}^{+}$ decreases with decreasing the ratio in case of UBL. It can be seen that mean temperature is slow to increase in case of SBL as shown in the right side of Fig. 9(b), but rapid increases of temperature can be observed in case of UBL.

Turbulent heat fluxes in streamwise and wall-normal directions are shown in Figs. 10 and 11, where the streamwise turbulent heat flux, $\overline{u\theta}$ clearly affects the Reynolds shear stress in the thermally-stratified turbulent boundary layer, because $\overline{u\theta}$ is contained in buoyancy term of the transport equation of Reynolds shear stress as $G_{uv} = Ri_{\delta_{2,\mathrm{in}}}\overline{u\theta}$. The wall-normal turbulent heat flux normalized by inner scale, $\overline{v\theta}^{+}$, increases in the downstream region in cases of both NBL and UBL. The wall-normal turbulent heat flux normalized by outer scale, $\overline{v\theta}^{*} = \overline{v\theta}/\bar{U}\Delta\Theta$, in case of NBL decreases in the downstream region, but $\overline{v\theta}^{*}$ in case of UBL increases in the downstream region. Thus, the different profiles of mean temperature between cases of NBL and UBL are obtained as shown in Fig. 9. On the other

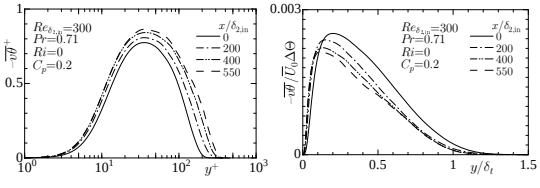

(a) Neutral stratification

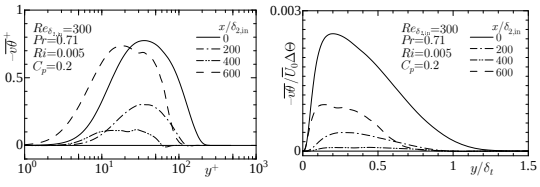

(b) Stable stratification

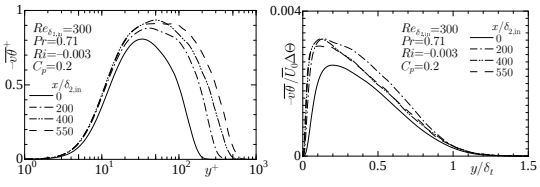

(c) Unstable stratification

Figure 10. Profiles of wall-normal turbulent heat flux; right side: inner scale, left side: outer scale

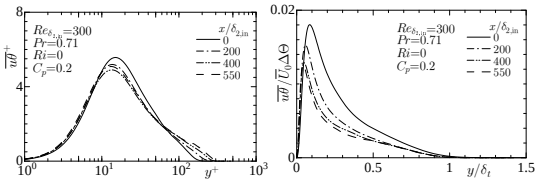

(a) Neutral stratification

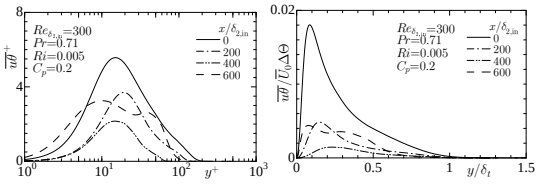

(b) Stable stratification

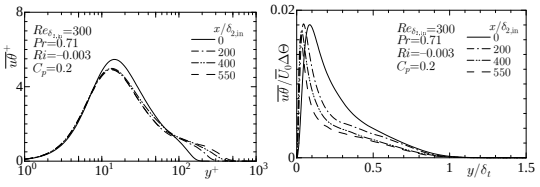

(c) Unstable stratification

Figure 11. Profiles of steamwise turbulent heat flux; right side: inner scale, left side: outer scale

hand, in case of SBL, $\overline{v\theta}^{+}$ one decreases in the downstream region, and then $\overline{v\theta}^{+}$ again increases. As for $\overline{v\theta}^{*}$ in case of SBL, $\overline{v\theta}^{*}$ almost vanishes at $x/\delta_{2,\mathrm{in}} = 400$, but it can be

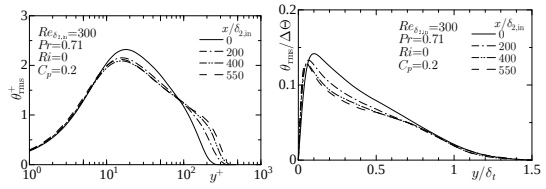

(a) Neutral stratification

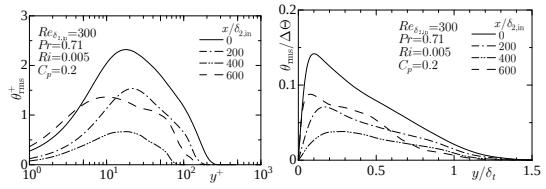

(b) Stable stratification

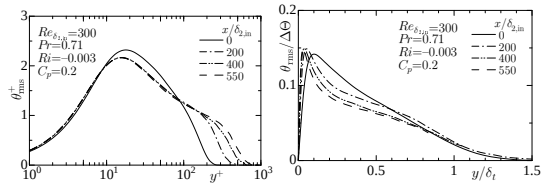

(c) Unstable stratification

Figure 12. Profiles of rms temperature fluctuation; right side: inner scale, left side: outer scale

seen that $\overline{v\theta}^*$ is re-generated as shown in the right side of Fig. 10(b). The streamwise turbulent heat flux is demonstrated in Fig. 11. It can be found that the streamwise turbulent heat flux normalized by inner scale, $\overline{u\theta}^+$, in cases of both NBL and UBL slightly decreases, and $\overline{u\theta}^*$ which is the streamwise turbulent heat flux normalized by outer scale, also decreases in cases of both NBL and UBL, but it can be seen that the near-wall $\overline{u\theta}^*$ increases in case of UBL. Since $\overline{u\theta}$ affects the Reynolds shear stress the thermally-stratified turbulent boundary layer as mentioned above, the increase of near-wall $\overline{u\theta}$ works on the enhancement of the Reynolds shear stress in case of UBL as shown in Fig. 5(c). In case of SBL, the behavior of $\overline{u\theta}$ is similar to the behavior of $\overline{v\theta}$ as shown in Fig. 10(b), but it can be observed that $\overline{u\theta}^*$ is not very small in comparison with $\overline{v\theta}^*$ at $x/\delta_{2,\mathrm{in}} = 400$. Since $\overline{u\theta}^*$ does not vanish in case of SBL, it is considered that the turbulence is maintained in case of SBL even if the APG affects.

Finally, the rms temperature fluctuation is shown in Fig. 12. In cases of both NBL and UBL, it can be seen that peak value of the rms temperature fluctuation normailized by inner scale, $\overline{\theta^2}^+$, decreases, and $\overline{\theta^2}^+$ increases in the outer region. Although $\overline{\theta^2}^*$ which is the rms temperature fluctuation normalized by outer scale only decreases in case of NBL, the increase of $\overline{\theta^2}^*$ near the wall and the decrease of $\overline{\theta^2}^*$ in the region around $0.1y/\delta_t \sim 0.5y/\delta_t$ can be observed in case of UBL. This different profiles strongly relate the profiles of the wall-normal turbulent heat flux as shown in Fig. 10, because the wall-normal turbulent heat is included in the production term of transport equation of $\overline{\theta^2}$. In case of SBL, it can be observed that $\overline{\theta^2}$ of both the normalizations remains in all regions, although the wall-normal turbulent heat flux almost vanishes at $x/\delta_{2,\mathrm{in}} = 400$. Thus, it is considered that terms of transport equation except for the production term act on the sustentation of $\overline{\theta^2}$.

CONCLUSIONS

DNSs of thermally-stratified turbulent boundary layers subjected to a non-equilibrium APG are carried out. DNS results clearly show the characteristic of thermally-stratified non-equilibrium APG turbulence flow. It is found that the mean velocity profiles normalized by inner scale of APG flow increase in case of SBL and decrease in case of UBL in the outer region due to the variation of friction coefficients, but decreases of free stream due to APG can be observed in both the cases. Also, characteristic profiles of turbulence are detected in the thermal field, in which decreases of mean temperature normalized by inner scale are observed in cases of NBL and UBL, although increases of mean temperature can be seen in case of SBL. Consequently, DNS results reveal that the turbulent characteristics of both cases of SBL and UBL with APG are different to those of the NBL having APG.

ACKNOWLEDGEMENT

This research was supported by a Grant-in-Aid for Scientific Research (C), 26420144, from the Japan Society for the Promotion of Science (JSPS).

REFERENCES

Araya, G. & Castillo, L. 2013 Direct numerical simulations of turbulent thermal boundary layers subjected to adverse streamwise pressure gradients. *Physics of Fluids (1994-present)* **25** (9).

Hattori, H., Hotta, K. & Houra, T. 2014 Characteristics and structures in thermally-stratified turbulent boundary layer with counter diffusion gradient phenomenon. *International Journal of Heat and Fluid Flow* **49**, 53 – 61.

Hattori, H., Houra, T. & Nagano, Y. 2007 Direct numerical simulation of stable and unstable turbulent thermal boundary layers. *International Journal of Heat and Fluid Flow* **28**, 1262–1271.

Hattori, H & Nagano, Y 2004 Direct Numerical Simulation of Turbulent Heat Transfer in Plane Impinging Jet. *International Journal of Heat and Fluid Flow* **25**, 749–758.

Houra, T. & Nagano, Y. 2006 Effects of adverse pressure gradient on heat transfer mechanism in thermal boundary layer. *International Journal of Heat and Fluid Flow* **27** (5), 967 – 976.

Lee, J. H. & Sung, H. J. 2008 Effects of an adverse pressure gradient on a turbulent boundary layer. *International Journal of Heat and Fluid Flow* **29** (3), 568 – 578.

Nagano, Y., Tagawa, M. & Tsuji, T. 1993 Effects of adverse pressure gradients on mean flows and turbulence statistics in a boundary layer. *Turbulent Shear Flows* **8**, 7–21.

Nagano, Y., Tsuji, T. & Houra, T. 1998 Structure of turbulent boundary layer subjected to adverse pressure gradient. *International Journal of Heat and Fluid Flow* **19** (5), 563 – 572.

Ohya, Y. 2001 Wind-tunnel study of atmospheric stable boundary layers over a rough surface. *Boundary-Layer Meteorology* **98**, 57–82.